REAL-TIME TIME IMPACT CONTROL OF A SOLID ROCKET MOTOR STAGE DURING LAUNCHER ASCENT

Solenn Hervouet * and Loïc Perrot **

* SCILOC Ingénierie, solenn.hervouet@sciloc.fr
** SCILOC Ingénierie, loic.perrot@sciloc.fr

Abstract

In this study, a method to control the fall-down area of a solid stage during launcher ascent is presented. The strategy is based firstly on the real-time estimation of the propulsive dispersions using a non-linear method. The impact control is included in more general launcher guidance. The algorithm is based on an analytical prediction-correction of the launcher trajectory and is sufficiently accurate after estimation of the propulsive dispersions to allow an effective limitation of the stage fall-down area. Finally the impact control efficiency and the launcher performance losses are evaluated statistically on a test case by large monte-carlo simulations. The results show that the re-entry conditions and the stage impact zone are controlled without excessive reduction of the launcher performance.

1. Introduction

Classically, to control the impact zone of a liquid stage, the powered flight phase of the stage is aimed at a predetermined orbit established in relation to safety requirements. The motor is shut down when the characteristics of the orbit, as estimated by the calculations of the on-board computer, are those of the target orbit. The impact zone area is thus defined by the guidance errors at stage separation and the debris dispersions after breakup at re-entry in the high atmosphere. Unlike liquid propulsion, a solid rocket motor cannot be switched off on request, so specific conditions cannot be reached precisely at burn out in order to limit the stage fall-down area. Despite this drawback, solid motors may bring certain benefits: a better long-term storage capability, a cheaper and simpler propulsion system, compactness, a higher reliability.

Various launch vehicles use stages with solid rocket motors: ASLV and PSLV (India), MINOTAUR and PEGASUS (OSC, United States), ATHENA (Lockheed Martin, United States), SHAVIT (Israel), VLS 4 (Brazil), START 1 (Russia), VEGA (Europe). They are small and medium launchers, but heavy launchers projects are underway as the future European Launcher Ariane 6 with the version "PPH" whose the two first stages using solid propulsion offer better cost competitiveness than a cryogenic core design.
By using upper solid stages, technical difficulties can arise as the limitation of the stage impact area after burn out. To mitigate this disadvantage an active control of the stage impact zone can be considered. To reach this objective, a guidance algorithm based on a prediction-correction scheme of the stage impact location combined with an estimator of the propulsive dispersions is proposed.
This preliminary study is a proof of concept, exploring the capabilities of a guidance method to limit the impact zone of a solid upper stage while preserving the launcher performance. In particular, this guidance method has to meet the following requirements:

- The guidance should be autonomous for on-board application
- The impact zone should stay within bounds, given propulsive, mass, atmospheric and aerodynamic dispersions,
- The launcher performance should be preserved,
- The guidance and control method should be simple and robust enough, as it would need to be implemented aboard a launcher.

2. The propulsive dispersions estimator

The control of the solid stage impact zone is based on the stage trajectory prediction until burnout. This prediction depends at first order on the velocity impulse remaining to deliver which is linked to the specific impulse (Isp) and the mass dispersions. So the estimation of the propulsive and mass dispersions is required for an accurate trajectory

prediction. As the classical extended Kalman filter fails on this problem due to high no linearity, we propose a new estimation approach based on a non linear identification method using only the longitudinal acceleration or the recorded ΔVs to estimate at each instant the propulsive parameters (flow rate (q), specific impulse (Isp) and incidentally the mass). It should be noted that to determine the dispersions on the specific impulse and mass from acceleration measures, an accurate estimation of the flow rate is needed first (see the thrust equation $T = qg_0Isp$ and $\Gamma = T/m$).
Thereafter, we define the following notation: index 0 refers to the propulsion model (or "nominal"); index 1 refers to real propulsion.

2.1. Flow rate estimation

Let $q_0(t)$ be the model flow rate function and $q_1(t)$ the dispersed flow rate function. We introduce a "time scaling" function $g(t)$ which reflects a shift of time relative to the "nominal" time due to the flow rate dispersion. We assume that this function is strictly increasing, positive, continuous and differentiable.

$$t : \text{(real time)} \longrightarrow t_0 = g(t) \ \text{(nominal time)}$$

We assume that g(t) follows the principle of mass conservation. Thus, at any given time, we must have:

$$\int_0^t q_1(v)dv = \int_0^{g(t)} q_0(u)du = \int_0^t g'(v)q_0\big(g(v)\big)dv$$

So, for $v>0$, the necessary condition must be verified:

$$q_1(v) = g'(v)q_0\big(g(v)\big) \qquad \textbf{(1)}$$

2.2. Specific impulse estimation

The specific impulse scattering is modelled using an additional function $l(t)$:

$$Isp_1(t)\big(1+l(t)\big) = Isp_0\big(g(t)\big) \qquad \textbf{(2)}$$

Using the relations above, the relation between the real and nominal accelerations is given by:

$$\Gamma_1(t)\ (1+l(t)) = \Gamma_0\big(g(t)\big)\cdot g'(t) \qquad \textbf{(3)}$$

2.3. Estimation principle

For given ordered measurement points (t_1, t_2 ... t_i ...t_{m+1}), the propulsive velocity measurements $\Delta V_1(t_i)$ are provided by an inertial navigation system (INS). The following relationship which expresses the link between the measurements ($\Delta V_1(t_i)$) and the thrust dynamic must be verified:

For i = 2, m+1:

$$\int_{t_1}^{t_i} \Gamma_1(u)(1+l(u))\,du = \int_{t_1}^{t_i} \Gamma_0\big(g(u)\big)\cdot g'(u)\,du = \int_{g(t_1)}^{g(t_i)} \Gamma_0(v)\,dv$$
$$\int_{t_1}^{t_i} \Gamma_1(u)(1+l(u))\,du = \Delta V_0(g(t_i)) - \Delta V_0(g(t_1)) \qquad \textbf{(4)}$$

The function $l(u)$ will be considered as linear on the interval $[t_1, t_{m+1}]$:

$$l(u) = l_1 + l_2 u \quad (u=t-t_1)$$

So, for each measurement $\Delta V_1(t_i)$ at t_i, using (4) we obtain:

$$\big(1+l(t_i)\big)\big(\Delta V_1(t_i) - \Delta V_1(t_1)\big) - l_2 \int_{t_1}^{t_i} \Delta V_1(u)\,du = \Delta V_0(g(t_i)) - \Delta V_0(g(t_1)) \qquad \textbf{(5)}$$

$\Delta V_0(g(t_i))$ is the nominal non gravitational velocity delivered until the reference time $g(t_i)$. ΔV_0 is a known function and can be tabulated. We suppose that an approximation of g(u) is known as a second degree polynomial on the measurement interval $[t_1, t_{m+1}]$:

$$g(u) = g_0 + u + a_1 + a_2 u + a_3 u^2 \quad (u = t - t_1) \qquad \textbf{(6)}$$

We propose to compute a correction of g given by:

$$\Delta g(u) = \Delta a_1 + \Delta a_2 u + \Delta a_3 u^2 \qquad \textbf{(6 b)}$$

By developing the right side of the equation (5) at first order with respect to (a_1, a_2, a_3) and rearranging we obtain a linear system:

$$Ax = b \qquad \textbf{(7)}$$

Where A is a (m x 3) matrix and $x = (\Delta a_1, \Delta a_2, \Delta a_3)$.

2.4. Computation process

If m > 3 the linear system (7) is overdetermined, a least mean square solution is computed by solving $A^T A\, x = A^T b$ Then we can improve $g(u)$ given by (6) with $\Delta g(u)$ (6 b) on the interval $[t_1, t_{m+1}]$:

$$a_i \leftarrow a_i + \Delta a_i \quad (i=1,3) \qquad \textbf{(8)}$$

Equation (5) is non linear wrt the parameters (a_i), so the solution of the linear system (7) must be used iteratively until the condition: $\Delta a_1 = \Delta a_2 = \Delta a_3 = 0$. The accuracy of the estimation is then given by:

$$E(x) = b^T b - b^T x \qquad \textbf{(9)}$$

which reflects the estimation error on ΔVis (in $(m/s)^2$). Finally a robust two-steps process is used to determine g(u) and l(u):

1. Resolution of (5) using the solution given by (7) and (8) with $l(u)$ fixed
2. $E(x)$ minimization by moving $l1$ et $l2$ while g(u) is fixed in the opposite direction of the gradient: $(\frac{\partial E(x)}{\partial l_1}, \frac{\partial E(x)}{\partial l_2})$.

If the two steps of the above process are iterated, we have verified that this process converges always to the minimum of $E(x)$ in few iterations with weak hypothesis on the initial conditions (for instance with $g(u)=g0+u$, $l(u)=0$).

When $E(x)$ reaches its minimum, the $g(u)$ and $l(u)$ functions are considered known, the real flow rate and specific impulse can be determined by (1) and (2) and are used for time-extrapolation and trajectory prediction. The predicted burnout time is given simply by the positive solution of a 2nd degree equation:

$$t_{f1} = g^{-1}(t_{f0})$$

where t_{f0} is the nominal burnout time.

2.5. Simulation and tests

The test case concerns the estimation of the propulsive dispersions of the third stage of the VEGA launcher (Z9).The Zefiro 9 (Z9) is a solid-fuel rocket motor (SRM), which equips the Vega launch vehicle's third stage. The nominal thrust profile (reference R6) is presented figure 1.

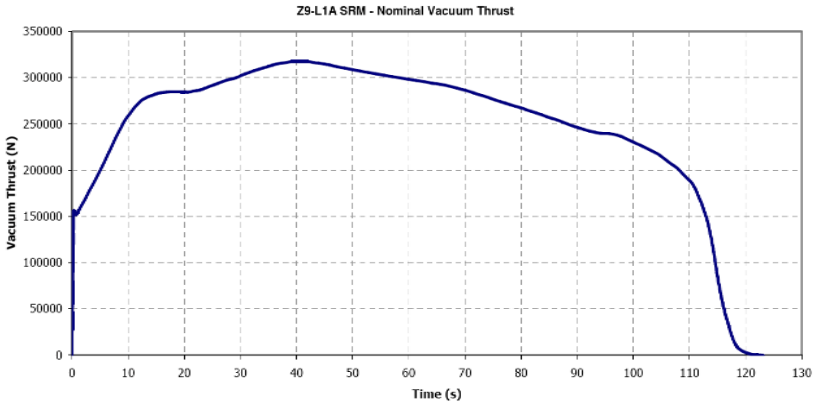

Figure 1: Z9 nominal vacuum thrust (from reference [R6])

The thrust envelope specification for the Z9 SRM is shown below (source ESA reference [R7]): upper and lower envelope (in red), nominal thrust prediction (in blue) and thrust reconstruction from SRM tests (in black). From the figure below, the maximum allowed dispersions with respect to the nominal case are estimated: ±3% for the burn time (or the flow rate), ±3.5%.for the thrust.

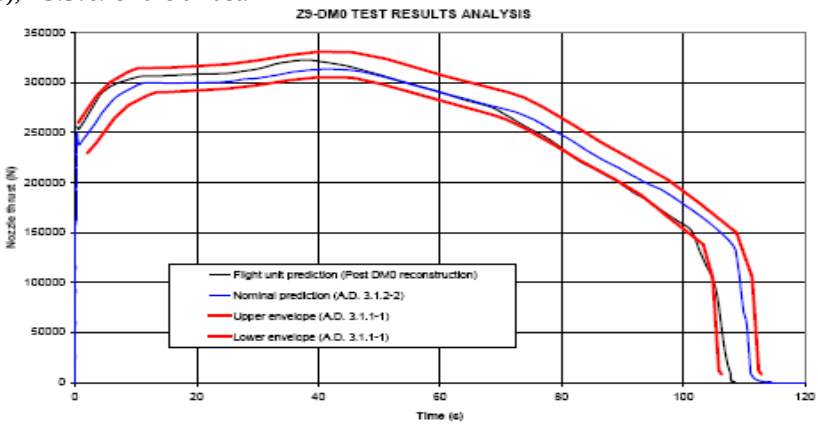

Figure 2 Z9 thrust envelope (from reference [R7])

To generate the real data recordings, INS errors (magnitude of the acceleration measurements errors: 1.5 10^{-4} g) are simulated with an INS velocity quantization effect. The non gravitational velocity measures (ΔV_i) are used. The ΔV_i measures are generated every 0.04s and the vector sampling length is fixed to 14s (m=350). The tests have shown that the flow rate and the specific impulse scatterings are observable and separable and can be identified in real time thanks to the computation process given at §2.4. Moreover any dispersion on the initial mass is identified and the burnout time can be predicted.

The accuracy is generally better than 0.5 % of the real flow rate and specific impulse. The CPU time is quite short: (single estimation) ~ 1 10^{-3} s (Intel Core 2 Duo T5870 2. GHz). The algorithm is simple and robust enough to allow onboard applications.

The figure 3 presents a result of the dispersions estimation. For this test case, the real dispersions are: dq= +3% varying to +3.8%, dIsp= -2% (dotted lines). The method converges after an observation period of 10 s. The estimation error E(x) remains close to zero until the beginning of the thrust tail-off (110s).

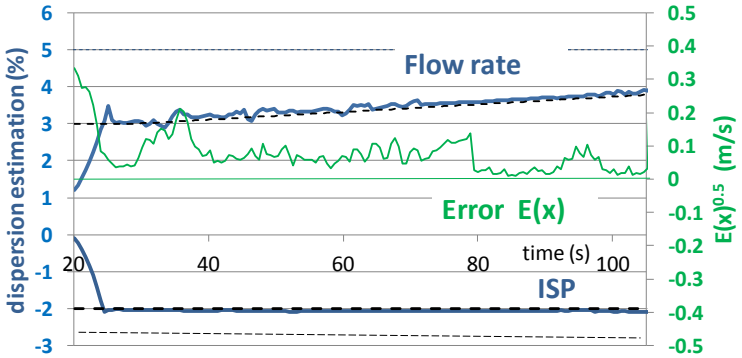

Figure 3 : Estimation of flow rate and Isp dispersions

3. The impact zone limitation strategy

3.1. Overview

As stated before, the strategy is in closed-loop. At each call of the guidance (typically every 2s), the control (written as the thrust orientation angles) is computed in four phases:

Phase 1: Dispersed flow mass / Isp estimation

Phase 2: Ballistic impact point prediction, with (q, Isp) estimation. To estimate the real impact, a fixed distance is considered between an impact point taking into account the drag and the predicted ballistic impact.

Phase 3: Analytic derivatives of the range wrt the control parameters computation.

Phase 4: Control correction by solving analytically a minimization problem with constraints.

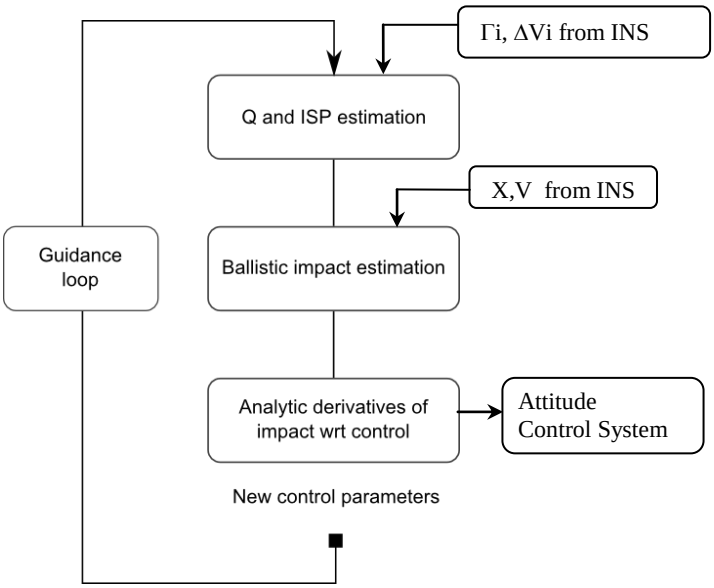

Figure 4 : Schematic diagram of the control of the stage fall-down area

3.2. Control frame and parameterization

- Guidance frame

The control is the thrust orientation during the powered stage flight. The thrust orientation is defined by two angles (θ,ψ) in the guidance frame. The guidance frame is inertial and is fixed at motor ignition. It axes (ξ, η, ζ) are defined by the aimed transfer orbit η : radius direction at nominal end position on the transfer orbit, ζ : opposite to the angular momentum, $\xi = \eta \times \zeta$.

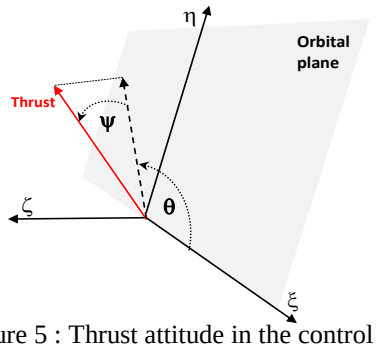

Figure 5 : Thrust attitude in the control frame

The angles θ and ψ determine the orientation of the thrust respectively in the trajectory plane and in the out-of-plane direction. This choice allows decoupling the equations of dynamics in the plane and out of the orbital plane. The angles are expressed as linear functions of time:

$$\theta(t) = \theta_0 + \dot{\theta} \times t \quad \text{Pitch (in-plane orientation)} \qquad \textbf{(10)}$$

$$\psi(t) = \psi_0 + \dot{\psi} \times t \quad \text{Yaw (out-of-plane orientation)}$$

This parameterization is near optimal for short boosts (see [R4]).

3.3. Simple Launcher guidance for upper stages

The first stages are flying in atmosphere. So, during this phase, the angle of attack must remain close to zero to avoid high structural loads. For these stages, the guidance law reduces to follow a pre-programmed attitude law based on gravity-turn (thrust attitude along the nominal trajectory). For the next stages flying out of the atmosphere, the thrust orientation is free, we will assume:

- A solid stage providing a major part of the necessary ΔV and for which the fall-down zone must be controlled.
- A reignitable stage (last stage using liquid propulsion) in charge firstly to reach a transfer orbit, and, after a ballistic phase and a second boost, to deliver the payload on the final orbit.

For this classical orbital maneuver strategy, particularly if the final orbit is circular, the transfer and final orbits need to be defined by only four orbital parameters (semi-major axis, eccentricity, inclination, ascending node (a, e, i, Ω)). We will suppose also that the orbital transfer requires only small corrections of the orbital plane (defined by i and Ω), then the control attitude during the boosts can be decoupled inside and outside the orbital plane.
The guidance is based on a prediction – correction of the orbital parameters reached at the end of each boost of the final stage.

- Orbit prediction

The prediction is carried out using the control parameterization (10). Writing second order Taylor developments of the control (considering the variations $\dot{\theta} t$ and ψ(t) as small) gives the following equations written in matrix form:

$$X(t_f) = X(t_0) + V(t_0) t_b - \frac{1}{2} \overline{\overline{g}}\, t_b^2 Id + M(\theta,\psi) \begin{bmatrix} S \\ Q \\ U \end{bmatrix}$$
$$V(t_f) = V(t_0) - \bar{g}\, t_b Id + M(\theta,\psi) \begin{bmatrix} L \\ I \\ P \end{bmatrix} \qquad \textbf{(11)}$$

t_0: current guidance time

t_b: time-to-go until burnout

t_f : final time (t_0 + t_b)

X: position vector

V: velocity vector

Id: identity vector

$\bar{g}$: mean gravity 1st order integral (with J2 and a third degree polynomial approximation)

$\overline{\overline{g}}$: mean gravity 2nd order integral (with J2 and a third degree polynomial approximation)

M: (3×3) matrix with coefficients computed from a second order Taylor development wrt (θ, ψ); the matrix M can be written like:

$$\mathbf{M} = \begin{bmatrix} A_0 & A_1 & A_2 \\ B_0 & B_1 & B_2 \\ a_2 & b_2 & c_2 \end{bmatrix}$$ with coefficients depending only on ($\theta_0, \dot{\theta}, \psi_0, \dot{\psi}$).

L, I, P, S, Q, U: 1st and 2nd order acceleration integrals of terms (Γ_0, Γ_0.t, Γ_0.t^2) computed with tabulated data and corrected with propulsive dispersions and mass estimations. The gravity integrals are written as third order polynomial approximations on the thrust arc.

Note: the prediction accuracy is increased if the relation (11) is cut in several segments of time.

- Orbit correction

- Thrust direction in the out-of-plane direction

ψ_0 and $\dot{\psi}$ are determined explicitly at each guidance call by writing the condition in the guidance frame using (11) (the components of the final state vector $(\vec{X},\vec{V})$ must be equal zero in the direction of the angular momentum of the target orbit):

$$(X(T_f).\zeta, V(T_f).\zeta) = (0,0)$$

- Thrust direction in the orbital plane

The derivatives: $\frac{\partial \vec{X}(t_f)}{\partial \vartheta_0}, \frac{\partial \vec{X}(t_f)}{\partial \dot{\vartheta}}, \frac{\partial \vec{V}(t_f)}{\partial \vartheta_0}, \frac{\partial \vec{V}(t_f)}{\partial \dot{\vartheta}}$ are computed using the relation (11) :

$$\frac{\partial M_i}{\partial \theta_0}=\begin{bmatrix} -B_0 & -B_1 & -B_2 \\ A_0 & A_1 & A_2 \\ 0 & 0 & 0 \end{bmatrix};\ \frac{\partial M_i}{\partial \dot{\theta}}=\begin{bmatrix} 0 & -B_0 & -B_1 \\ 0 & A_0 & A_1 \\ 0 & 0 & 0 \end{bmatrix}$$

Using (11) and the derivatives of M above, the derivatives computation of $(\vec{X},\vec{V})$ wrt $(\theta_0,\dot{\theta})$ is straightforward.

$\frac{\partial \vec{X}(t_f)}{\partial t_b}$, $\frac{\partial \vec{V}(t_f)}{\partial t_b}$ are also computed easily as M is time-independent.

Using the derivatives of the state vector we can compute the derivatives of the apogee and perigee altitudes with respect to (θ_0, $\dot{\theta}$, t_b).

Pitch and time-to-go corrections

By using the more practical parameter ΔV instead t_b (equivalence is given by $d\Delta V=\Gamma(t_f)dt_b$), the control corrections at each guidance call are solution of the system:

$$\begin{aligned} &\frac{\partial hapo}{\partial \theta_0}d\theta_0+\frac{\partial hapo}{\partial \dot{\theta}}d\dot{\theta}+\frac{\partial hapo}{\partial \Delta V}d\Delta V=\Delta hapo \\ &\frac{\partial hperi}{\partial \theta_0}d\theta_0+\frac{\partial hperi}{\partial \dot{\theta}}d\dot{\theta}+\frac{\partial hperi}{\partial \Delta V}d\Delta V=\Delta hperi \end{aligned} \qquad \textbf{(12)}$$

Where $\Delta hapo$, $\Delta hperi$[1] are the corrections required on the altitudes of apogee and perigee.

The system (12) is overdetermined. Therefore, we solve firstly this system considering $d\dot{\theta}$ =0 and, to stay in the linear validity domain of the parameters variation, with the constraints:

$$|d\theta_0| \le d\theta_0 \max,\ \left|d\Delta\vec{V}\right| \le d\Delta V \max \qquad \textbf{(13)}$$

(Note: Values of $\Delta hapo$ and $\Delta hperi$ are automatically reduced if the system (12) with the constraints (13) has no solution)

Optimisation of the Launcher performance by ΔV minimization

After correction of (ΔV, θ_0) with $d\Delta V$ and $d\theta_0$ solutions of (12) with the constraints (13), ΔV can be minimized by moving the solution $(\theta_0,\dot{\theta},\Delta V)$ in the plane tangent to the constraints (12) and by varying firstly the additional parameter $\dot{\theta}$. Thus, the problem depends only on $d\dot{\theta}$ and can be stated as:

$$\min_{\dot{\theta}} \frac{\partial \Delta V}{\partial \dot{\theta}}d\dot{\theta}$$

The following constraints must be verified with any variation of $\dot{\theta}$:

$$\begin{aligned} &\frac{\partial hapo}{\partial \theta_0}d\theta_0+\frac{\partial hapo}{\partial \dot{\theta}}d\dot{\theta}+\frac{\partial hapo}{\partial \Delta V}d\Delta V=0 \\ &\frac{\partial hperi}{\partial \theta_0}d\theta_0+\frac{\partial hperi}{\partial \dot{\theta}}d\dot{\theta}+\frac{\partial hperi}{\partial \Delta V}d\Delta V=0 \end{aligned}$$

Where: $d\Delta V=\frac{\partial \Delta V}{\partial \dot{\theta}}d\dot{\theta}$; $d\theta_0=\frac{\partial \theta_0}{\partial \dot{\theta}}d\dot{\theta}$ and

$$|d\theta_0|=\left|\frac{\partial \theta_0}{\partial \dot{\theta}}d\dot{\theta}\right| \le d\theta_0 \max$$
$$|d\Delta V|=\left|\frac{\partial \Delta V}{\partial \dot{\theta}}d\dot{\theta}\right| \le d\Delta V \max$$
$$\left|d\dot{\theta}\right| \le d\dot{\theta} \max$$

The derivatives $\frac{\partial \theta_0}{\partial \dot{\theta}}$, $\frac{\partial \Delta V}{\partial \dot{\theta}}$, with the condition of constraints verification (equation (12) with a second member equal to zero), verify the relations:

[1] For circular orbits, the variations of the semi-major axis and eccentricity (Δa, Δe) will be preferably used in the system (12) instead ($\Delta hapo$, $\Delta hperi$).

$$\frac{\partial \theta_0}{\partial \dot{\theta}} = \frac{1}{\Delta}\left(-\frac{\partial hperi}{\partial \Delta V}\frac{\partial hapo}{\partial \dot{\theta}} + \frac{\partial hapo}{\partial \Delta V}\frac{\partial hperi}{\partial \dot{\theta}}\right)$$

$$\frac{\partial \Delta V}{\partial \dot{\theta}} = \frac{1}{\Delta}\left(\frac{\partial hperi}{\partial \theta_0}\frac{\partial hapo}{\partial \dot{\theta}} - \frac{\partial hapo}{\partial \theta_0}\frac{\partial hperi}{\partial \dot{\theta}}\right)$$

$$\Delta = \frac{\partial hapo}{\partial \theta_0}\frac{\partial hperi}{\partial \Delta V} - \frac{\partial hperi}{\partial \theta_0}\frac{\partial hapo}{\partial \Delta V}$$

Guidance initialisation

The efficiency of this very simple guidance algorithm depends nevertheless on the control initialization. The initialisation of the guidance control (ΔV, $\theta(t)$, $\psi(t)$) can be based on the open-loop control of the optimized nominal trajectory given during the mission preparation.
Nevertheless, for orbital transfer between near-circular orbits (say eccentricity less than 0.1), the ΔV can be approximated by the classical Hohman transfer and the thrust attitude by the hypothesis of tangential thrust. In this case, using this initial control, tests have shown a good convergence to the solution.

3.4. Ballistic impact prevision

We express the range as an angle α between the current position and the position of the impact ($\alpha=\alpha_1+\alpha_2$).

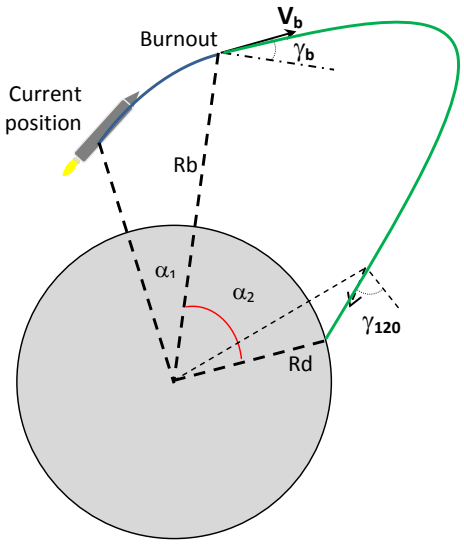

Figure 6 : Parameters of the Ballistic range prevision

The control strategy is built from an analytic prediction of this range. We have to predict first the position/velocity of the launcher at stage burn-out, and the ballistic impact given this position/velocity. The prediction of the state vector at burn-out is performed thanks to the equations (11).

Keplerian impact prediction

The range α_2 can be explicitly expressed as a function of the radius (R_b), the velocity (V_b), the path angle (γ_b) at burnout and the orbit parameters (a, e) using classical conics formulas (see reference [R3] for details).

3.5. Analytic derivatives

The derivatives are computed in two phases. The parameters (R_b, V_b, γ_b) at stage burnout are found using (11). Then, we can express first the derivative of α_2 wrt (R_b, V_b, γ_b) (see [R3]). Using (11) and the derivatives of M wrt the control parameters, the derivatives of (R_b,V_b,γ_b) wrt the control parameters are computed. Using both sets of derivatives, we can then write the total derivatives of the range angle (α) wrt the control parameters.

3.6. Control correction

The path angle at burnout (γ_b) acts directly on the propellant consumption of the upper stage. The variable γ_b is linked directly to the path angle at 120km (γ_{120}). By controlling γ_{120}, we can control both the propellant consumption

of the upper stage and the atmospheric re-entry. Therefore we impose that γ_{120} lies in a certain interval. For that, the derivatives of the control wrt the path angle at 120km are used, according the situation, to minimize or to maximize the path angle at re-entry. The problem is written as a set of equations and constraints that depend on the pitch control variations.
The formulas for the prediction and the derivatives are valid only for first and second variations of the control, so the control is constrained to limited variations.
The control correction will be performed by solving the problem:

$$\begin{aligned} &\mathbf{min(or\,max)}\ (e\,\delta\theta_0 + f\,\delta\dot{\theta}) \\ &(\delta\theta_0,\delta\dot{\theta}) \\ &a\,\delta\theta_0 + b\,\delta\dot{\theta} = k\,\delta\alpha \\ &\left|\delta\theta_0 + \delta\dot{\theta}\,t_b\right| < D_M \\ &\theta_{0m} \le \delta\theta_0 \le \theta_{0M} \\ &\dot{\theta}_m \le \delta\dot{\theta} \le \dot{\theta}_M \end{aligned} \qquad \textbf{(14)}$$

a and *b* are the derivatives of the range and *e* and *f* are the derivatives of the path angle at 120km. $\delta\alpha$ is the range correction to stay in the authorized fall-down area, *k* is a proportionality coefficient set to gradually correct the impact range . D_M is the maximum correction allowed on $\delta\theta$ during the time span. We also impose bounds on $\delta\theta_0$ and $\delta\dot{\theta}$ to limit the control variations.
The problem will be a minimization problem if γ_{120} is near its maximum allowed; a maximization problem if γ_{120} is near its minimum allowed. The problem (14) is solved explicitly at each guidance call by a deterministic algorithm. If no solution of this problem exists, a maximal value of $\delta\alpha$ is recomputed to comply with the bounds.
ψ_0 and $\dot{\psi}$ are determined by the condition of orbital plane conservation at t_b: $(\vec{X}(t_b).\zeta, \vec{V}(t_b).\zeta) = (0,0)$.

4. TEST CASE

The test case considered for the study is the VEGA Launcher and its reference mission (polar earth orbit, (PEO mission, see reference [R9])). Vega is a launch vehicle comprising three stages with solid rocket motors: the P80 first stage, the Zefiro-Z23 second stage, the Zefiro-Z9 third stage
The fourth stage, AVUM, ensures mission versatility, injecting the payload(s) into final orbit generally through a transfer orbit. The baseline performance set for Vega is the PEO mission which consists to inject from Kourou 1500. kg into a circular polar orbit at 700 km altitude, inclined 90° to the equator.

Launcher data

Table 1 Launcher data

Stages	Inert mass (kg)	Propellant mass (kg)	Vacuum Isp (s)	tc (s)
P80	7431	88365	280	107
Z23	1845	23906	289	72
Z9	1423	10115	293	120
Avum	662	550	315.5	694
Fairing	560			
Payload	1500			

The Launcher data come from various open sources. They have been extracted mainly from the Vega User's manual of Arianespace (reference [R8]). Some data (Z9 inert mass, fairing mass and Avum inert mass) have been updated by more recent documents (references [R9], [R6], [R10]). The inter-stages masses are included in the stages inert mass in the table above. The Launcher aerodynamic data come from document reference [R12] (aerodynamic drag coefficient for Vega). The SRMs thrust laws considered here are those presented in reference [R7]. These data may differ from official reference data, but we think that they are sufficient to test our method.

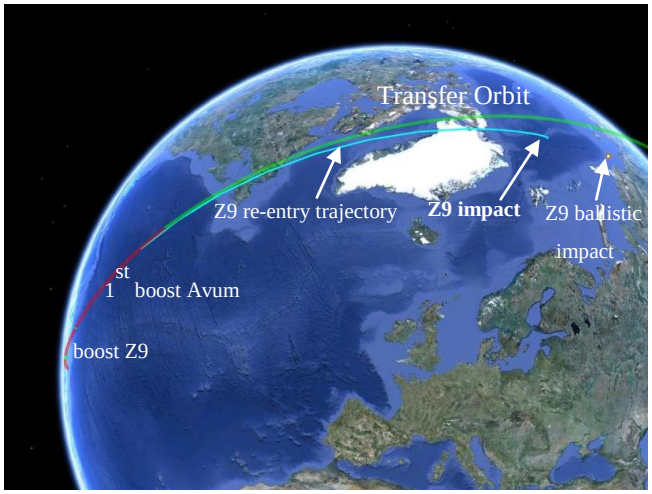

Figure 7 Nominal trajectory of VEGA (PEO mission)

Mission scenario for the PEO mission

During the flight of the two first stages (P80, Z23) in atmosphere, the angle of attack is kept near zero. After Z9-Z23 separation and a short ballistic phase, the 3rd stage is ignited and the fairing is jettisoned when the conventional heat flux comes below a certain threshold (1135 w/m^2). After fairing jettisoning, the launcher attitude is free and the launcher guidance aimed a transfer orbit reached at the end of the first boost of Avum. Then the final stage (Avum) follows a ballistic trajectory before a re-ignition and a 2nd boost to circularise the orbit.

For the test case, the parameters of the transfer orbit resulting of a pre-optimisation are:

Tableau 2: Transfer orbit parameters

Apogee Altitude	Perigee Altitude	Inclination	Argument of perigee	Ascending node
692.5 km	163 km	89.95 d°	20.5 d°	0.83°

For the VEGA reference mission (PEO orbit) and in nominal conditions (without dispersions), considering a drag coefficient of 6.510^{-3} ([2]), the Z9 stage falls in the Arctic Ocean a thousand km beyond Greenland. The ballistic impact is located forward at approximately 1200 km from the impact point with drag (see figure 7).

Note: According to our model assumptions (launcher data, flight sequential, guidance), we cannot certify that our results are representative of a real trajectory of the VEGA Launcher.

4.1. The Monte-Carlo computation process

To compute the possible Z9 impact zone, we use a Monte-Carlo process based on a quasi-random process more accurate than the standard monte-carlo method (Sobol quasi-random generator (reference [R1]). We suppose that the dispersions which affect the Launcher follow a Gaussian Law. The following table lists the dispersed parameters and their standard deviations [3]:

Table 3: Monte-Carlo parameters

	Propulsive dispersions	
Stage	Flow rate Std. Dev.	Isp Std. Dev.
P80	2 %	0.5%
Z23	2%	0.5%
Z9	1%	0.5%
Avum (1st boost)	2.5%	0.3%
Avum (2nd boost)	2.5%	0.3%

[2] See references [R2] and [R5] for estimation of the drag coefficient of stage debris
[3] The standard deviations of the propulsive laws are estimated from the documents in references ([R7] and [R13])

Other dispersions	
Drag coefficient (Std. Dev.)	Dispersion profile wrt mach
Atmospheric density	Dispersion profile wrt altitude

We consider a dispersed atmosphere (model GRAM10 reference [R11]) for which a standard deviation of the atmospheric density is given wrt altitude.

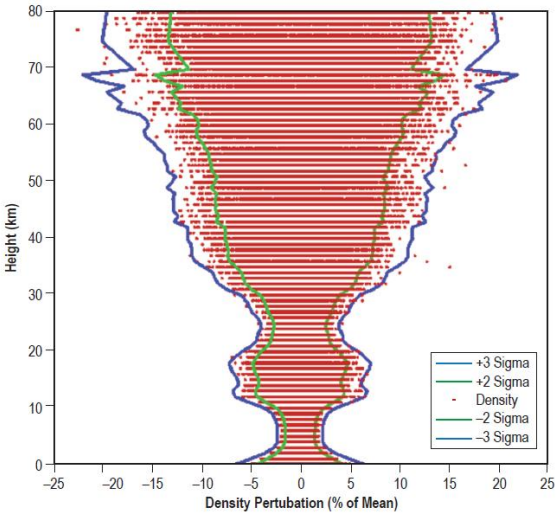

Figure 8: Density perturbation model (reference [R11])

4.2. Debris footprint model

This study is not aimed at modelling precisely the Z9 debris re-entry. We have chosen to simplify the computations by integrating the re-entry trajectory taking into account the drag force with a constant drag coefficient (SCx/m) and the earth J2 effect (see references [R2] [R5]) for drag coefficient values of the pieces of a space vehicle after breakup). No lift was modelled nor any breakup phenomenon.
The correction strategy is based on analytic derivatives of the ballistic impact wrt control parameters. Obviously, the real impact location differs from the ballistic impact. Monte-Carlo results will show that for a given test case, there is a more or less constant offset between the two, the path angle and relative velocity at 120km being the most influent parameters. A "virtual" ballistic target has been accordingly assigned to the range correction algorithm.

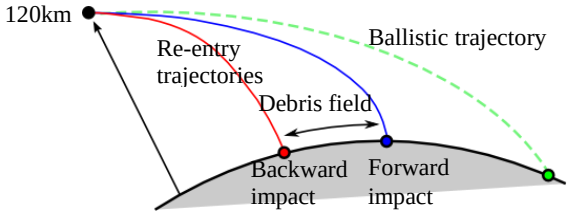

Figure 9 : Debris footprint modelling

5. Computation results

To obtain a sufficiently accurate statistical fall down zone, 100 000 Monte-Carlo runs have been computed.

5.1. Monte Carlo results without impact control

As a reference, we computed first a full Monte Carlo without activating the control of the Z9 impact zone. The Launcher thrust attitude is computed with the guidance algorithm defined in § 3.3. For all the simulations, the final orbit has been reached accurately without any propellant depletion (accuracy better than 0.5 km for the semi-major axis (a), less than 0.004° for i and Ω), thus demonstrating the efficiency and the robustness of the guidance algorithm.

Results

Table 1: impact zone characteristics and propellant consumption (nominal guidance without impact control)

Parameter	Value
Max. Undershoot distance [4]	-2458 km
Undershoot distance at probability 10^{-3}	-2017 km
Undershoot distance at probability 10^{-4}	-2300 km
Max Overshoot Distance [5]	4619 km
Overshoot distance at probability 10^{-3}	2985 km
Overshoot distance at probability 10^{-4}	3641 km
Statistical Avum propellant consumption (probability 10^{-2})	470.5 kg

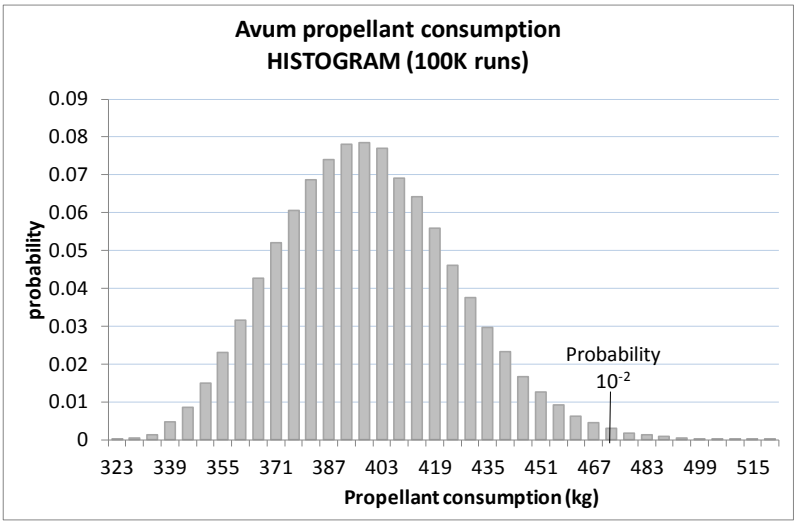

Figure 10 Avum propellant consumption (Histogram)

The figure 10 shows the distribution of Avum propellant consumption. The statistical propellant consumption is moderate and leaves enough propellant reserve to compensate the dispersions and to proceed to Avum de-orbit.

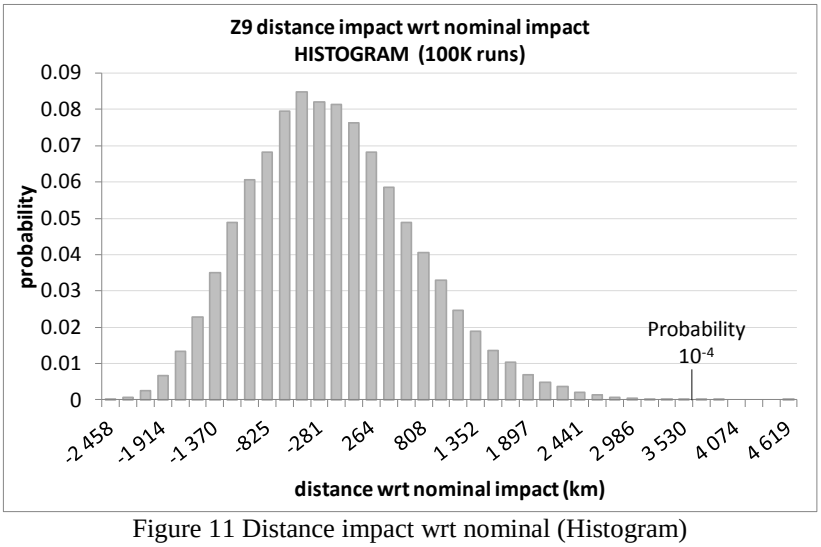

Figure 11 Distance impact wrt nominal (Histogram)

[4] Undershoot distance : distance from nominal impact, the impact is behind the nominal impact (negative value by convention)

[5] Overshoot distance : distance from nominal impact, the impact is beyond the nominal impact (positive value)

The figure 11 shows the impact distribution of the Z9 stage. For this monte-carlo simulation (100 000 runs), the fall-down zone stretches over 7100 km; the forward part of the distribution presents a very flat tail suggesting possible important overshoot impact distances for low probability.

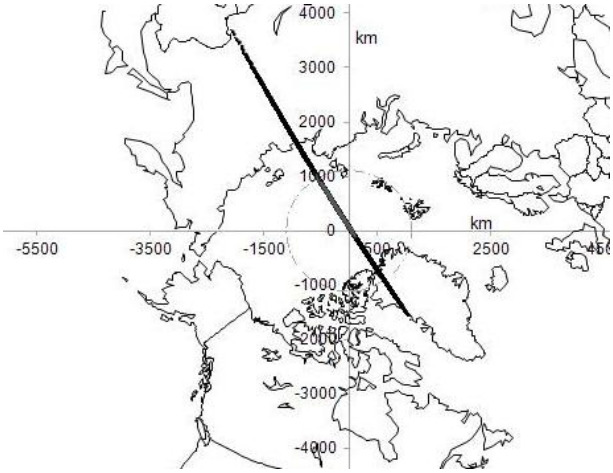

Figure 12 Z9 statistical Z9 fall-down zone over the Arctic Ocean (100 000 runs)

The figure 12 visualizes the statistical fall down zone, an important part of the fall down zone lies beyond the coasts.

5.2. Monte Carlo results with impact control

The same full Monte Carlo simulation (100 000 runs) is performed now with impact control. The authorized Z9 fall-down area is defined with respect to a maximum distance between the Z9 ballistic impact point which results from the simulation with dispersions and the ballistic impact point of the nominal trajectory (without dispersions). The maximum distance depends on the nature of the impact (undershoot, overshoot):

Maximum undershoot ballistic impact point: 700 km
Maximum overshoot ballistic impact point: 500 km

Impact control strategy

If the ballistic impact is outside the above limits, the nominal launcher guidance is interrupted and the impact control is activated. The range impact is corrected thanks to the algorithm defined at §3.6. According to the discussion at § 3.6, to control both the propellant consumption of the upper stage and the atmospheric re-entry, the following strategy is applied (§ 3.6):

- if $\gamma_{120} > -2°$, γ_{120} is minimized and the ballistic range impact corrected
- if $-4° < \gamma_{120} \leq -2°$, the Z9 ballistic range impact is corrected only
- if $\gamma_{120} < -4°$, γ_{120} is maximized and the ballistic range impact corrected

Results

For all the simulations, the final orbit has been reached accurately: the errors on the orbit parameters of the final orbit are less than 0.7 km for the semi-major axis, less than 0.005° for i and Ω.

Table 2: impact zone characteristics and propellant consumption with impact control

Parameter	Value
Max. Undershoot distance	-690 km
Undershoot distance at probability 10^{-3}	-553 km
Undershoot distance at probability 10^{-4}	-608 km
Max Overshoot Distance	867 km
Overshoot distance at probability 10^{-3}	651 km
Overshoot distance at probability 10^{-4}	740 km
Statistical Avum propellant consumption (probability 10^{-2})	477.8 kg

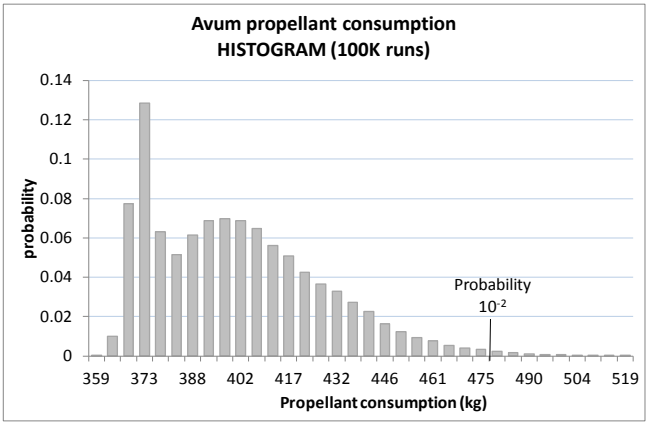

Figure 13 Avum propellant consumption with impact control

The figure 13 shows the distribution of the Avum propellant consumption. The fuel consumption increases slightly (+7.3 kg at a probability of 0.01), the histogram shows a flatter distribution.

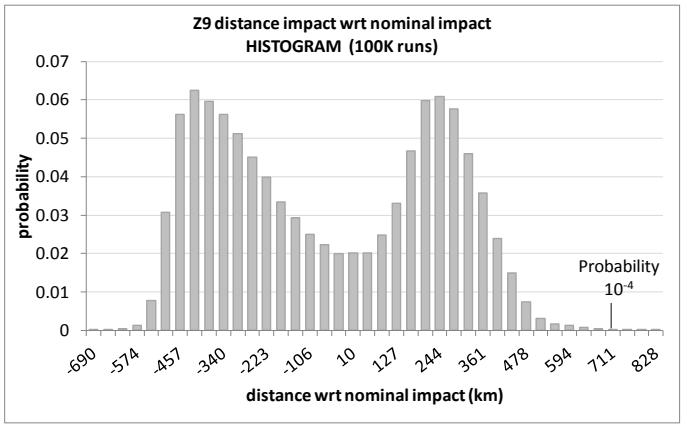

Figure 14 Distance impact distribution with impact control

The negative distances in figure 14 are for undershoot impacts. We can check on the figure 14 that the impact control is effective: the length of the Z9 fall-down zone is now reduced to 1500 km. The ballistic impact zone was constrained to [-700 km, 500 km]. Taking to account the drag, the impact zone is found here to [-690 km, 828 km]. Because the method manages only the ballistic impact zone, a great part of this difference can be explained by a non constant deviation between the ballistic impact and the real impact with drag, and also by the error of the propulsive dispersions estimation leading to a threshold violation, especially for the extreme overshoot cases. The tail distribution is quite short for the overshoot or undershoot impact zones. So, it can be expected than that the extreme impact points at very low probability lie at a reasonable distance of the nominal impact point.

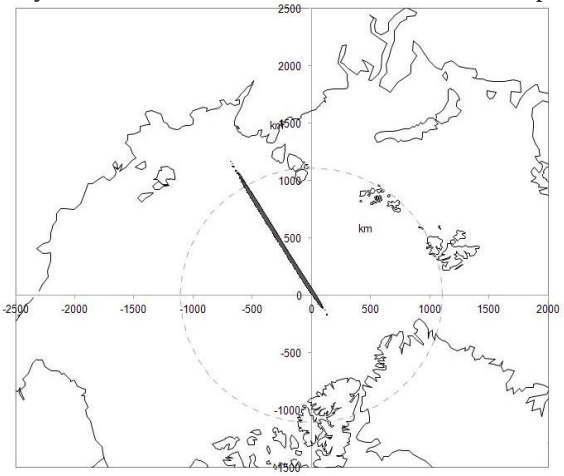

Figure 15 Z9 statistical fall-down zone with impact control (100 000 runs)

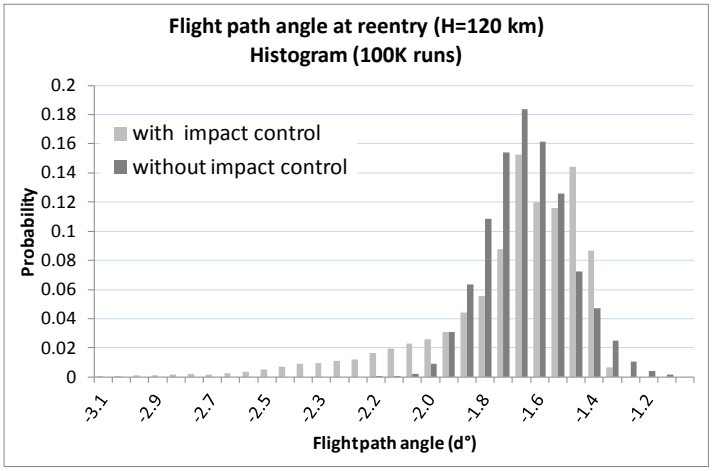

Figure 16 Flight path angle at re-entry with and without impact control

On the figure above, we can see that the impact control strategy decreases the path angle at re-entry and generally shifts the values of the path angle to lowest values.

Table 3: Probability comparison for low path angle at re-entry

Probability [γ_{120} > -1.3°]	
Without impact control	With impact control
4%	0.7%

6. Conclusion

The ability of our method to limit the fall-down zone of a solid stage during the Launcher ascent is demonstrated. The solid dispersion estimator is also proven efficient and can have application for other space vehicle guidance. In addition, the impact control method increases only slightly the propellant consumption of the final stage in charge to deliver the payload while reducing significantly the fall-down zone and ensuring a direct re-entry by lowering the flight path angle at re-entry. Therefore the impact control method presented here does not penalize the Launcher performance (at least for the study case presented here).

We can conclude also that the simplicity of the impact control method for solid stages coupled with a robust Launcher guidance allows envisaging an onboard application in real time. However, this is still a preliminary work and following issues need to be addressed:

- Tests on others missions and launchers,
- Global strategy accuracy and Launcher performance optimisation,
- Quantification and effect of the dispersions of a solid motor at tail-off

7. References

[R1] Bratley P. and Fox B.L. (1988). Implementing Sobol's quasirandom sequence generator, *ACM Transactions on Math. Software 14*, 88-100

[R2] Mrozinski R. B. (2003). NASA Pre-event Debris Footprint Estimates for the Deorbit of Space Station MIR, Nasa Johnson Space Center, USA.

[R3] Siouris G. M., 2004. Missile Guidance and Control Systems, Springer.

[R4] "Autonomous Optimal Deorbit Targeting", Donald J. Jezewski, AAS/AIAA 1991

[R5] Trajectory design and control for the Compton gamma ray observatory re-entry. Hoge, Vaughn Flight Mechanics symposium 2001

[R6] Vega Launch system- Final Preparation for qualification flight A. Neri VEGA-IPT ESRIN Vega Program Status JPC 11 for STTC.ppt

[R7] Vega Launcher F. Serraglia VEGA-IPT ESRIN November 2008

[R8] VEGA User's Manual Arianespace (2006)

[R9] VEGA satellite Launcher AVIO VEGA quartino_new_m.indd - zefiro_9_77.pdf

[R10] VEGA status and qualification flight preparation S. Bianchi, R. Lafranconi, M. Bonnet ESRIN

[R11] The NASA MSFC Earth Global Reference Atmospheric Model – 2010 Version NASA/TM – 2011 -216467

[R12] Global and Local Multidisciplinary Design Optimization of Expendable Launch Vehicles. F Castellini, A Riccardi, M Lavagna Report 11-09 Bremen Universität Zentrum für Technomathematik December 2011

[R13] The (successful) experience of The Maiden Flight of Vega, in parallel to the worth mission to lift Lares PG Lasagni, P Bellomi ELV Fiat Avio PPT presentation (Post-flight analyses, SRM thrust laws envelopes)